Origin of Ferromagnetism in Cyano-Bridged Compounds Containing d^1 Octacyanometallates**

Liviu F. Chibotaru,* Vladimir S. Mironov, and Arnout Ceulemans

Giant-spin molecular clusters have attracted much attention in recent years in connection to the design of single-molecule magnets (SMM) based on the phenomenon of blocking of magnetization at low temperatures.[1] One of the requirements for the polynuclear clusters to become a molecular magnet is the high value of the ground-state spin. In this respect, cyano-bridged clusters seem to be promising. Their structural and magnetic properties can easily be tuned by combining $[M(CN)_n]^{m-}$ mononuclear-complex building blocks. As a result, a large variety of cyano-bridged compounds of different dimensionality ranging from clusters to three-dimensional (3D) networks have been synthesized.[2] Among them molecular magnets with high magnetic-ordering temperatures have been obtained on the basis of bimetallic and mixed-valence transition metal cyanides of the Prussian blue family.[3]

Recently, two new groups of heterometallic cyano-bridged compounds have been reported.[4–7] The first corresponds to clusters with fully capped cubane structure (Figure 1) and unusually high ground-state spin. Three compounds of this structure are known to date: they are **1** with $S = 51/2$,[4], **2** with $S = 39/2$,[5] and **3** with $S = 12$.[6]

$[Mn^{II}\{Mn^{II}(MeOH)_3\}_8(\mu\text{-}CN)_{30}\{Mo^{V}(CN)_3\}_6]\cdot 5\,MeOH\cdot 2\,H_2O$ **1**

$[Mn^{II}\{Mn^{II}(EtOH)_3\}_8(\mu\text{-}CN)_{30}\{W^{V}(CN)_3\}_6]\cdot 12\,EtOH$ **2**

$[Ni^{II}\{Ni^{II}(MeOH)_3\}_8(\mu\text{-}CN)_{30}\{Mo^{V}(CN)_3\}_6]\cdot 17\,MeOH\cdot H_2O$ **3**

The second group includes the 3D networks **4** with a ground state spin per formulae unit of $S = 11/2$ (M = Mn), $S = 9/2$ (M = Fe), and $S = 7/2$ (M = Co).[7]

$[Nb^{IV}\{(\mu\text{-}CN)_4M^{II}(H_2O)_2\}_2]\cdot 4\,H_2O$ (M = Mn, Fe, and Co) **4**

[*] Dr. L. F. Chibotaru, Prof. Dr. A. Ceulemans
Department of Chemistry
Katholieke Universiteit Leuven
Celestijnenlaan 200F, 3001 Leuven (Belgium)
Fax: (+32) 16-32-79-92
E-mail: Liviu.Chibotaru@chem.kuleuven.ac.be
Dr. V. S. Mironov
Institute of Crystallography
Russian Academy of Sciences
Leninskii prosp.59 117333 Moscow (Russia)

[**] Financial support by the Belgian National Science Foundation and Flemish Government under the Concerted Action Scheme, the ESF programme on molecular magnets, the Russian Foundation for Basic Research (Grant No. 01-02-32210), and the INTAS Grant 00-00565 are gratefully acknowledged. The authors thank Professor Silvio Decurtins and the members of his group for stimulating discussions and for sending us the structural data on the niobium compound prior the publication, and Dr. Høgni Weihe for useful discussions. We also thank Ken Somers for the help with the Figures.

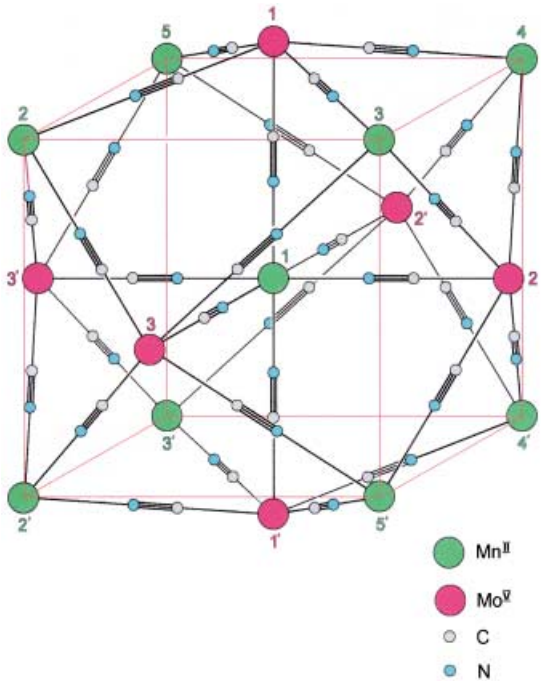

Figure 1. The structure of the $Mo^{V}_6Mn^{II}_9(\mu\text{-}CN)_{30}$ core of the cluster **1** (symmetry group C_2) which contains three nonequivalent molybdenum sites. A similar core is found in **2** (symmetry group S_6), which contains six equivalent tungsten sites, and in **3**.

A common structural feature of **1**–**4** is that they contain octacyanocoordinated Mo^{V}, W^{V}, and Nb^{IV} d^1 metal ions in a high-valent state coupled to low-valent transition metal ions by cyanide bridges. Another distinctive feature is that all the compounds except **2** are ferromagnetic. This result is surprising since no orthogonality of the magnetic orbitals is expected from the structure of these compounds.

Herein, we elucidate the reasons for ferromagnetism in **1**, **3**, and **4** and for the different magnetic behavior of **2**. It is found that these properties are mainly because of the specific symmetry properties of the magnetic orbitals at the octacoordinate ions.

There are two types of coordination for octametallates in the above compounds (Figure 2). The coordination of molybdenum and tungsten in **1**, **2**, and **3** has the geometry close to that of a trigonal dodecahedron (orange frame in Figure 2a). This geometry can be obtained from the cube by compression of one of the two interpenetrating tetrahedra and elongation of the other one, so that the C_4 rotation axis becomes S_4 (green arrow in Figure 2a) and the symmetry lowers from O_h to D_{2d}. In the idealized dodecahedron corresponding to the closest ligand packing, the eight ligands are equidistant from the central metal ion and form polar angles of 36.9° and 69.5° with the S_4 axis. According to the structural data, all the Mo^{V} and W^{V} sites have a nearly regular dodecahedral coordination with angular distortions of less than 3° in **1** and 5° in **2**, and Mo–C and W–C bonds being equal to 2.14 Å within 0.02 Å.[4, 5]

Figure 3a shows the ground d orbital, d_1, on the Mo1 site in **1** calculated with the angular overlap model (AOM). It is predominantly represented by the $d_{x^2-y^2}$ orbital with a small

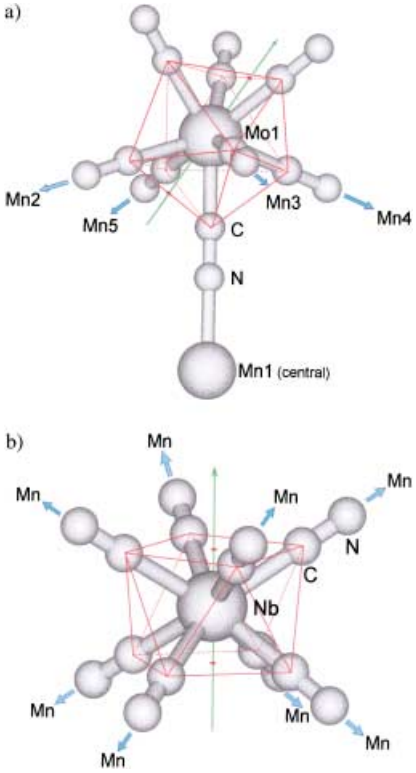

Figure 2. The structure of the octacoordinate metal fragments in the cluster **1** (a) and the compound **4** (b). The fragment in (a) is isostructural to the W site in **2** and the Mo site in **3**. Blue arrows indicate the bridging to the nearest neighbor manganese ions. Green arrows are the main symmetry axes of the orange frames.

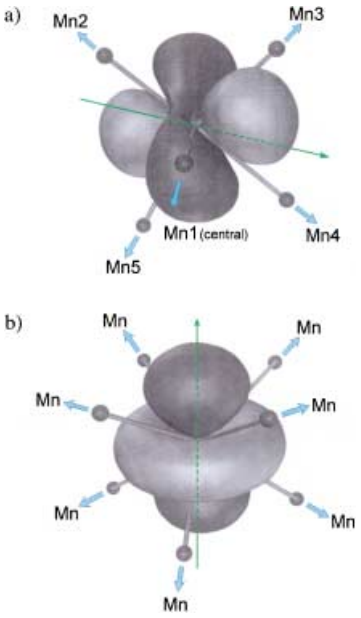

Figure 3. Ground ligand-field orbital d_1 (magnetic orbital) on the Mo1 site in **1** (a) and the Nb site in **4** (b). The arrows have the same meaning as in Figure 2.

admixture of the d_{z^2} orbital arising from small deviations from the strict D_{2d} symmetry of the dodecahedron (in which the z axis coincides with the S_4 axis and x and y with the two C_2 axes). The same is true for the other two non-equivalent molybdenum sites in **1**. Since all the Mo-C-N groups are almost linear, the one σ-and two π-orbital components of the carbon atoms into the corresponding molecular orbitals of the cyanide unit will be directed along and perpendicular to the Mo–C bonds, respectively. Simple symmetry analysis shows that in a D_{2d} dodecahedron the orbital $d_{x^2-y^2}$ is strictly orthogonal to the eight s orbitals pointing from the ligands. This orthogonality is almost fulfilled at all the molybdenum centers in **1** because of the small distortions from the idealized dodecahedral geometry. Indeed, Figure 3a shows that all the Mo–C bonds lie close to the nodal plane of the orbital d_1. An estimation of the overlap of this orbital with s and p cyanide orbitals can be assessed from the projections of d_1 orbital onto the d_σ and d_{π_x}, d_{π_y} components, defined with respect to a given Mo-C-N line (left side of Figure 4).

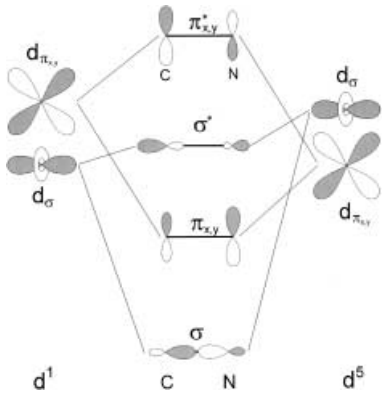

Figure 4. Definition of the d_σ, d_{π_x}, and d_{π_y} orbitals on the 4d(M) and 3d(M′) sites for a given metal pair M-(CN)-M′ (π_y-type orbitals lie in the plane perpendicular to the drawing). The two basic electron-transfer pathways (σ and π) through the cyanide bridge are outlined by the thin oblique lines. The corresponding transfer parameters describe the electron transfer in the chains: $\beta_\sigma = d_\sigma(M)$-σ*,σ(CN)-$d_\sigma(M')$, $\beta_\pi \equiv \beta_{\pi_x} = \beta_{\pi_y} = d_{\pi_x}(M)$-π*,π(CN)-$d_{\pi_x}(M')$.

The square of these components, $F_\sigma(d_1,l_i)^2$ and $F_{\pi_x}(d_1,l_i)^2 + F_{\pi_y}(d_1,l_i)^2$, which define the destabilization of the d_1 orbital by the jth cyanide ligand,[8] are listed in Table 1. The σ overlap is negligibly small compared with the π overlap for all the octametallate sites in the clusters **1** and **2**. The same can be expected for the Mo^V centers in **3** which is structurally similar.

In the 3D networks of **4**, the coordination geometry of the Nb^{IV} ions is close to square antiprismatic (orange frame in Figure 2b). Four ligands are equivalent within the upper and lower planes, but the Nb–C distances and polar angles of upper and lower ligands with respect to the C_4 axis of the antiprism (green arrow in Figure 2b) are somewhat different, so that the symmetry lowers from D_{4d} to C_{4v}. In this geometry, the lowest ligand field orbital d_1 on the niobium ion will be of pure d_{z^2} type (Figure 3b).[9] Noteworthy is that the σ overlap of the d_1 orbital with the cyanide orbital vanishes exactly at the cubic polar angle $\theta_{cub} = 54.7°$. The actual polar angles in the $Nb(CN)_8^{4-}$ fragments, $\theta_2 = 58.2°$, $\pi - \theta_1 = 57.5°$, are very close the closest packing angle $\theta_{c.p.} = 59.2°$ and differ by only a few degrees from θ_{cub}. As a result the directions of the Nb–C bonds for all eight cyanide ligands pass very close to the nodal cones of the d_1 orbital (Figure 3b). That is why in these

  0044-8249/01/11323-4562 $ 17.50+.50/0

Table 1. Angular overlap factors for the ground magnetic orbital d_1 of octametallate sites with respect to σ and π bonds in Mo-CN-Mn, W-CN-Mn, and Nb-CN-Mn pairs in compounds **1**, **2**, and **4**.

Metal pair (i, j)		$F_\sigma(d_1, l_j)^2 \times 10^4$	$F_{\pi_x}(d_1, l_j)^2 + F_{\pi_y}(d_1, l_j)^2$
Mo1	Mn1	10.1	0.331
	Mn2	4.8	0.900
	Mn3	119.0	0.788
	Mn4	57.5	0.442
	Mn5	0.1	0.899
Mo2	Mn1	3.9	0.275
	Mn3	3.3	0.949
	Mn4	61.8	0.723
	Mn4′	8.5	0.951
	Mn5′	59.3	0.541
Mo3	Mn1	0.9	0.279
	Mn2	0.5	0.397
	Mn2′	28.5	0.892
	Mn3	42.5	0.914
	Mn5′	0.01	0.941
W	Mn1	1.2	0.265
	Mn2	1.4	0.940
	Mn3	138.0	0.617
	Mn4	86.3	0.636
	Mn5	10.8	0.944
Nb	Mn1	44.8	0.616
	Mn2	69.7	0.602

octametallates the σ overlap of d_1 is very small too, which is also confirmed by small $F_\sigma(d_1, l_j)^2$ values in Table 1. We can therefore conclude that in the whole series the lowest ligand-field orbital d_1 at the octacyanometallate sites has a *negligible σ overlap* with all the orbitals of the bridging cyanides.

These results have important implications for the magnetism of our compounds. Since d_1 accommodates one electron it also corresponds to a single magnetic orbital at the octametallate centers in **1**–**4**, while the 3d centers contain several magnetic orbitals the unpaired electrons of which form a high-spin ground state (Figure 5). The magnetic coupling (or

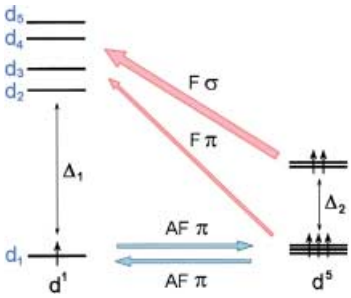

Figure 5. Scheme of the antiferromagnetic (AF; blue) and ferromagnetic (F; pink) kinetic contributions to the superexchange in the (Mo^{V},W^{V},Nb^{IV})-Mn^{II} metal pairs. The arrows indicate the direction of the electron transfer in each contribution.

exchange interaction) between the spins of two centers is described by the conventional Heisenberg spin Hamiltonian $H = -2JS_1S_2$. The spin–spin coupling constant J involves antiferro- and ferromagnetic contributions which are further analyzed within the framework of the kinetic exchange theory.[10]

Figure 5 shows the kinetic contributions to the exchange interaction between spins $S = 1/2$ and $S = 5/2$ in an Mo^{V}-(CN)-Mn^{II} pair. The antiferromagnetic kinetic part [Eq (1)],[10]

$$J_a = -\frac{2}{5}\sum_{\lambda=\pi_x,\pi_y} t_{1\lambda}^2\left(\frac{1}{E_{1\to\lambda}}+\frac{1}{E_{\lambda\to 1}}\right) \quad (1)$$

contains the contributions of the electron transfer from the molybdenum magnetic orbital (d_1) to the manganese magnetic orbitals (d_λ) through the π orbitals of the cyanide bridge and vice versa, described by the transfer parameters $t_{1\lambda}$, with electron promotion energies $E_{1\to\lambda}$ and $E_{\lambda\to 1}$, respectively. Note that in Equation (1) a negative J value favors an antiferromagnetic ground state.

The ferromagnetic kinetic part [Eq. (2)],[10, 11] includes contributions of the electron transfer from the manganese

$$J_f = \frac{2}{5}\sum_{i=2}^{5}\sum_{\lambda=\sigma,\pi_x,\pi_y}\frac{t_{i\lambda}^2}{E_{\lambda\to i}}\frac{I_{1i}}{E_{\lambda\to i}} \quad (2)$$

magnetic orbitals to the molybdenum empty d orbital. I_{1i} describes the intra-atomic exchange interaction between the electron in the magnetic orbital d_1 and the transferred electron to the empty excited orbital d_i on the molybdenum site. The terms $t_{i\lambda}$ are parameters of the electron transfer between three of the manganese half-filled orbitals (λ), involved in the σ, π_x, and π_y through-bridge electron-transfer pathways, and four empty orbitals on the molybdenum site ($i = 2,\ldots5$); $E_{\lambda\to i}$ are the corresponding electron promotion energies. Since the high-spin manganese(II) ion is spherically symmetric, for each cyanide bridge the d orbitals can be defined in such a way that three of them will coincide with d_σ, d_{π_x}, and d_{π_y} orbitals in Figure 4.

The resulting exchange parameter is the sum of J_a and J_f.[12] The competition between these two contributions can be presented in a more simple form. First, the transfer parameters $t_{i\lambda}$ in Equations (1) and (2) for each ligand (l_i) can be expressed by only two independent parameters, β_σ and β_π (Figure 4), multiplied by the corresponding projection coefficients $F_\lambda(d_1, l_j)^2$. Second, one can neglect the ligand-field splitting of the excited d orbitals which is small compared to the leading electron-repulsion contribution into $E_{i\to\lambda}$. By introducing the notations $U_1 = E_{1\to\pi}$, $U_2 = E_{\pi\to 1}$ for Mo→Mn electron transfer between the lowest orbitals and vice versa, the promotion energies for the electron transfer between π and σ orbitals of the manganese to the empty d orbitals of molybdenum become $U_2 + \Delta_1$ and $U_2 + \Delta_1 - \Delta_2$, respectively. Δ_1 and Δ_2 are ligand-field splitting energies on the d^1 and d^5 ions (Figure 5). Third, the parameters I_{1i} in Equation (2) are replaced by their average over the excited d_i orbitals, I.[14] Fourth, using the summation rules for the projection coefficients [Eq. (3)] one can eliminate the summations over the excited d orbitals of the molybdenum site in Equation (2) by expressing them through the relationship given as (4) and (5) below.

$$\sum_{i=1}^{5} F_\sigma(d_i, l_j)^2 = 1, \quad \sum_{i=1}^{5}(F_{\pi_x}(d_i, l_j)^2 + F_{\pi_y}(d_i, l_j)^2)^2 = 2 \quad (3)$$

$$F_\sigma(d_i, l_j)^2 \quad (4)$$

$$C_\pi \equiv F_{\pi_x}(d_1, l_j)^2 + F_{\pi_y}(d_1, l_j)^2 \quad (5)$$

Neglecting the small quantity $F_\sigma(d_i, l_j)^2$ (Table 1) we can finally write down the criterion for ferromagnetism, $J_f > -J_a$, as Equation (6)

$$\frac{\beta_\sigma^2 I}{(U_2 + \Delta_1 - \Delta_2)^2} + (2 - C_\pi) > C_\pi \beta_\pi^2 \left(\frac{1}{U_1} + \frac{1}{U_2}\right) \quad (6)$$

Ligand-field analysis gives $\Delta_1 = 5$ eV and $\Delta_2 = 1.5$ eV, a lowest estimate for $U_1 = 10$ eV.[10a] Given the large difference in valences of molybdenum and manganese ions, U_2 is expected to be 2–3 times smaller than U_1, while I has a value around 1 eV.

The critical ratio of the σ and π transfer parameters for the onset of ferromagnetism under the least-favorable condition $C_\pi = 1$ (Figure 6) decreases with the decrease of U_2 and the increase of I (relative to U_1) and for the estimated values of parameters is found in the range $3.5 < |\beta_\sigma/\beta_\pi| < 4.5$. Hence for ferromagnetism the σ transfer between the manganese magnetic orbitals and the molybdenum empty d orbitals (Figure 5) should be several times stronger than the π transfer between the magnetic orbitals of two metal sites.

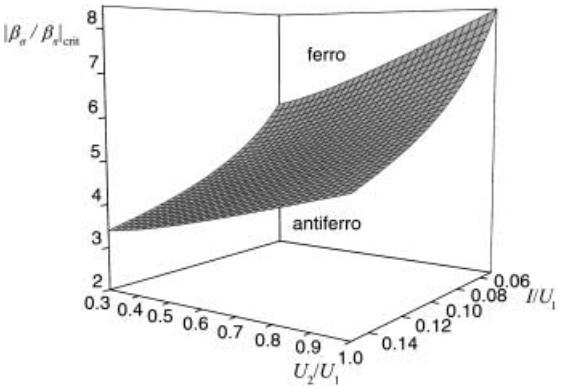

Figure 6. Critical ratio of β_σ and β_π transfer parameters for the onset of ferromagnetism in $4d^1$–$3d^5$ metal pairs.

This is clearly the case for the cyanide bridges where strong covalent admixtures into d_σ are naturally expected because of a close energy position of the σ*(CN) orbital (Figure 4) to the valence d shells of both metal sites. The overlap of the manganese d_σ magnetic orbital with some of molybdenum empty orbitals through the cyanide bridge is significant (Figure 7). As additional evidence, a much stronger σ covalency, compared to the π one, was found in $Cr(CN)_6^{3-}$ ions where about 15% covalent admixture was calculated for the $3d_\sigma(e_g)$ orbitals and only 1% for the $3d_\pi(t_{2g})$ orbitals.[15] Finally, our direct estimations of the transfer parameters in the M-(CN)-M′ pairs within the extended Hückel approach give $|\beta_\sigma/\beta_\pi|$ values ranging from 2 to 3. On the other hand it should be noted that Figure 6 presents an upper estimate for the critical value of $|\beta_\sigma/\beta_\pi|$. Indeed, this value should be additionally scaled by a factor $\approx\sqrt{C_\pi}$, which is always smaller than unity (Table 1) because $C_\pi = 1$ would correspond to a perfect overlap of d_1 with the π orbitals of the cyanide. The neglected ferromagnetic contribution from the direct (potential) exchange,[10, 13] will further reduce the critical value of $|\beta_\sigma/\beta_\pi|$.

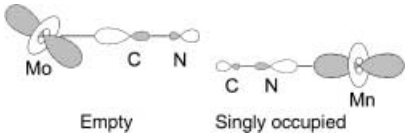

Figure 7. The manganese d_σ magnetic orbital and the molybdenum d_2 empty orbital. The latter also contains admixtures of the cyanide π orbitals (not shown).

The above considerations apply directly to the explanation of ferromagnetic exchange in the Mo–Mn and Nb–Mn pairs of **1** and **4**. Passing to $M = Fe^{II}$, Co^{II} in **4** will merely quench some π antiferromagnetic transfer channels since addition of one and two electrons to the manganese d^5 shell results in the occupation of the d_π orbital. This leads to the increase of ferromagnetism in these compounds. The strongest ferromagnetic effect is expected when M has a completely filled d_π shell and unpaired electrons in the d_σ orbitals. Indeed, the latter do not overlap with the magnetic orbital d_1 at the octametallate site and the antiferromagnetic contribution vanishes [$t_{1\lambda} = 0$ in Eq. (1)]. This is the case for the Mo^V-(CN)-Ni^{II} pairs in **3** which indeed shows the highest ferromagnetic J value of the series.[6] As for the antiferromagnetism in **2**, it can have several causes. A more diffuse 5d shell of tungsten atoms compared to the 4d shell of molybdenum results in smaller intra-atomic exchange interaction (smaller I) and larger $|\beta_\sigma/\beta_\pi|$ critical ratio in Figure 6 for the tungsten ion. Besides, the transfer parameters themselves are expected to change when passing from **1** to **2** because of their high sensitivity to the positions of the d levels on the octametallate sites.

In summary, the exchange interaction in the cyanide complexes with the core $[M_6^V M_9'^{II}(\mu\text{-}CN)_{30}]$, M = Mo, W, M′ = Mn, Ni, and 3D networks $[Nb^{IV}\{(\mu\text{-}CN)_4 M'^{II}(H_2O)_2\}]$, M′ = Mn, Fe, Co, are analyzed within the Anderson superexchange theory. It is found that the magnetic orbital of each octametallate in these compounds exhibits an almost perfect orthogonality to the σ orbitals of the eight neighboring cyanide ligands despite having a quite different coordination geometry. As a result the antiferromagnetic contribution to the exchange can only be determined by the π transfer between magnetic orbitals, while the ferromagnetic kinetic contribution mainly arises from the σ transfer from the 3d ions. Two factors, the relatively low electron-promotion energy from 3d to 4(5)d ions and the large σ transfer parameter, which exceeds several times the π one, push the balance between the two kinetic exchange contributions towards ferromagnetism. This proposal explains why the compounds **1** and **4** are ferromagnetic in spite of the open π antiferromagnetic channel for electron transfer between magnetic orbitals. In the Mo–Ni cluster **3** the ferromagnetism is additionally stabilized because of absence of the d_π unpaired electrons on the nickel sites.

Received: July 16, 2001 [Z17525]

[1] a) P. D. W. Boyd, Q. Li, J. B. Vincent, K. Folting, H. R. Chang, W. E. Streib, J. C. Huffman, G. Christou, D. Hendrickson, *J. Am. Chem. Soc.* **1988**, *110*, 8537–8539; b) A. Caneschi, D. Gatteschi, R. Sessoli, A. L. Barra, L. C. Brunel, M. Guillot, *J. Am. Chem. Soc.* **1991**, *113*, 5873–5874; c) R. Sessoli, D. Gatteschi, A. Caneschi, M. Novak,

  0044-8249/01/11323-4564 $ 17.50+.50/0

Nature **1993**, *365*, 141 – 143; d) R. Sessoli, H. L. Tsai, A. R. Schake, S. Wang, J. B. Vincent, K. Folting, D. Gatteschi, G. Christou, D. Hendrickson, *J. Am. Chem. Soc.* **1993**, *115*, 1804 – 1816; e) D. D. Awschalom, D. P. Di Vincenzo, *Phys. Today* **1995**, *48*, 43; f) E. D. Dahlberg, J.-G. Zhu, *Phys. Today* **1995**, *48*, 34.

[2] a) T. Mallah, C. Auberger, M. Verdaguer, P. Veillet, *J. Chem. Soc. Chem. Commun.* **1995**, 61 – 62; b) S. M. El Fallah, E. Rentschler, A. Caneschi, R. Sessoli, D. Gatteschi, *Angew. Chem.* **1996**, *108*, 2081 – 2083; *Angew. Chem. Int. Ed. Engl.* **1996**, *35*, 1947 – 1949; c) A. Scuiller, T. Mallah, M. Verdaguer, A. Nivorozhkin, J.-L. Tholence, P. Veillet, *New J. Chem.* **1996**, *20*, 1 – 3; d) J. L. Heinrich, P. A. Berseth, J. R. Long, *J. Chem. Soc. Chem. Commun.* **1998**, 1231 – 1232; e) S. Ferlay, T. Mallah, R. Quahès, P. Veillet, M. Verdaguer, *Inorg. Chem.* **1999**, *38*, 229 – 234; f) T. Mallah, A. Marvilliers, E. Rivière, *Philos. Trans. R. Soc. London Ser. A* **1999**, *357*, 3139 – 3158.

[3] a) W.-D. Griebler, D. Babel, *Z. Naturforsch. B* **1982**, *37*, 832; b) V. Gadet, T. Mallah, I. Castro, M. Verdaguer, P. Veillet, *J. Am. Chem. Soc.* **1992**, *114*, 9213; c) T. Mallah, S. Thiebaut, M. Verdaguer, P. Veillet, *Science* **1993**, *262*, 1554 – 1557; d) S. Ferlay, T. Mallah, R. Quahès, P. Veillet, M. Verdaguer, *Nature* **1995**, *378*, 701; e) S. M. Holmes, G. S. Girolami, *J. Am. Chem. Soc.* **1999**, *121*, 5593.

[4] J. Larionova, M. Gross, M. Pilkington, H. Andres, S. Stoeckli-Evans, H. U. Güdel, S. Decurtins, *Angew. Chem.* **2000**, *112*, 1579 – 1583; *Angew. Chem. Int. Ed*. **2000**, *39*, 1605 – 1609.

[5] Z. J. Zhong, H. Seino, Y. Mizobe, M. Hidai, A. Fijishima, S.-I. Ohkoshi, K. Hashimoto, *J. Am. Chem. Soc.* **2000**, *122*, 2952 – 2953.

[6] F. Bonadio, M. Gross, H. Stoeckli-Evans, S. Decurtins, *Mid-Term Conference on the ESF Programme "Molecular Magnets"* (Davos) **2001**, P22.

[7] P. Franz, L. Keller, M. Pelkington, J. Ensling, S. Decurtins, *Mid-Term Conference on the ESF Programme "Molecular Magnets"* (Davos) **2001**, H4.

[8] A. B. P. Lever, *Inorganic Electronic Spectroscopy*, 2nd ed., Elsevier Science, Amsterdam, **1984**, chap. 1.

[9] J. R. Perumareddi, A. D. Liehr, A. W. Adamson, *J. Am. Chem. Soc.* **1963**, *85*, 249 – 259.

[10] a) P. W. Anderson, *Phys. Rev.* **1959**, *115*, 2 – 13; b) P. W. Anderson in *Magnetism*, *Vol. 2* (Eds.: G. T. Rado, H. Suhl), Academic Press, New York, **1963**, chap. 2.

[11] J. B. Goodenough, *Magnetism and Chemical Bond*, Interscience, New York, **1963**, chap. 5.

[12] It also includes the contribution from the direct (potential) exchange,[10,13] not considered here for simplicity.

[13] O. Kahn, *Molecular Magnetism*, VCH, Weinheim, **1993**, chap. 8.

[14] J. S. Griffith, *The theory of Transition Metal Ions*, Cambridge University Press, Cambridge, **1971**, p. 84.

[15] L. G. Vanquickenborne, L. Haspeslagh, M. Hendrickx, J. Verhulst, *Inorg. Chem.* **1984**, *23*, 1677 – 1684.

"Cap-Tag"—Novel Methods for the Rapid Purification of Oligosaccharides Prepared by Automated Solid-Phase Synthesis**

Emma R. Palmacci, Michael C. Hewitt, and Peter H. Seeberger*

The automated solid-phase synthesis of oligopeptides[1] and oligonucleotides[2] is now routine and has made a major impact on the biochemistry and biotechnology of these biopolymers. Attempts to automate the synthesis of carbohydrates, the most complex class of biopolymers, on solid phase[3] and by computer-assisted planning of solution syntheses[4] have only recently been disclosed. While automated solid-phase synthesis greatly simplifies the assembly process by eliminating the time-consuming purification of intermediates, it is this very feature that often makes the final purification challenging. The removal of sequences deficient by just one unit ($n-1$ products) stemming from incomplete couplings at any stage of the synthesis can be very difficult.

Automated solid-phase synthetic protocols for peptides[5] and nucleic acids[2] often incorporate a capping step in the synthetic cycle to minimize the accumulation of $n-1$ products. Further improvements of this technique are based on the introduction of a capping agent that functions as a unique handle to aid in the purification of the final product.[6]

With the advent of combinatorial chemistry and parallel synthesis, several methods for the expedient purification of a variety of compounds have been reported. Scavenging resins allow byproducts or excess reagents to be removed by reaction of the unwanted moieties with a support-bound functional group, followed by filtration.[7] Affinity labels such as biotin or oligohistidine exploit noncovalent binding and have been extensively used for the rapid purification of tagged biomolecules[8] and synthetic compounds[9] by affinity chromatography. Most recently, the unique behavior of highly fluorinated molecules has been utilized to separate molecules containing a fluorous tag from nonfluorinated compounds by extraction with fluorous solvents or by chromatography on fluorous silica gel.[10]

Here we describe two novel capping-and-tagging (cap-tag) methods to aid in the purification of oligosaccharides

[*] Prof. Dr. P. H. Seeberger, E. R. Palmacci, M. C. Hewitt
Department of Chemistry
Massachusetts Institute of Technology
Cambridge, MA 02139 (USA)
Fax: (+1) 617-253-7929
E-mail: seeberg@mit.edu

[**] Financial support from the donors of the Petroleum Research Fund, administered by the ACS (ACS-PRF 34649-G1), Merck (Predoctoral Fellowship for E.R.P.), Boehringer-Ingelheim (Predoctoral Fellowship for E.R.P.), and the NIH (Biotechnology Training Grant for M.C.H.) is gratefully acknowledged. Funding for the MIT-DCIF Inova 501 was provided by the NSF (Award CHE-9808061). Funding for the MIT-DCIF Avance (DPX) 400 was provided by the NIH (Award 1S10RR13886-01). We thank Silicycle (Quebec City, Canada) for the generous gift of fluorous silica gel and isocyanate silica gel scavenger resin. We thank Dr. O. Plante for helpful discussions and help with the automated oligosaccharide synthesizer.

Supporting information for this article is available on the WWW under http://www.angewandte.com or from the author.